

To appear in January 1999 A.J.

M SUBDWARFS: THE POPULATION II LUMINOSITY FUNCTION

JOHN E. GIZIS¹ AND I. NEILL REID²

Palomar Observatory, 105-24, California Institute of Technology, Pasadena, California 91125
 e-mail: gizis@stratford.phast.umass.edu, inr@astro.caltech.edu

ABSTRACT

We present results of a study of very low mass halo stars. Using a sample of proper motion stars identified from plate material taken as part of the first and second Palomar Sky Surveys, we measure the space density, metallicity distribution, and kinematics of the Population II M subdwarfs. Our overall luminosity function is in good agreement with previous analyses of the space density of nearby very-low-mass halo subdwarfs, and confirms the discrepancy between local analyses and the space densities inferred from deep HST starcounts. We show for the first time that both the metallicity distribution and kinematics of late-type halo subdwarfs are consistent with those of their higher mass metal-poor counterparts. Dividing our sample by abundance, we find no evidence that the mass function of field halo stars is dependent upon metallicity. We provide data for three nearby subdwarfs that may merit additional observations.

Subject headings: Galaxy: halo — stars: low-mass, brown dwarfs — stars: luminosity function, mass function — stars: Population II

1. Introduction

Long-lived low-mass stars are a local relic of the earliest stages of the Galaxy's formation. Dubbed the Population II in contrast to the disk Population I, these stars make up the Galactic halo (sometimes called spheroid). Although comprising only a very small fraction of the stars in the Galaxy, Population II stars provide one of the most important records of Galactic history.

The Population II luminosity function is of particular interest since its derivation is a requirement in most studies of the stellar mass function. Determination of the stellar mass

¹Current Address: Department of Physics and Astronomy, LGRT 532A, University of Massachusetts, Amherst MA 01003-4525

²Visiting Research Associate, Carnegie Institute of Washington

function as function of Galactic epoch and metallicity provides significant constraints upon the theory of star formation. Evolution of the mass function with time or metallicity might be expected since conditions in star-forming clouds were likely much different in the protoGalaxy (c.f. Zinnecker 1995). Moreover, since halo brown dwarfs have faded far below the threshold for even near-infrared detection, the form of the subdwarf mass function near the hydrogen-burning limit represents the most effective technique (in the absence of gravitational lensing detections) for estimating the Population II dark matter contribution.

Despite the intuitive simplicity of the process of counting stars to determine the luminosity function, there have substantial disagreements between different studies in both the normalization and slope of the luminosity function (see the review of Mould 1996). Two recent surveys have measured the space density of very-low-mass Population II stars, the M subdwarfs. Counts of faint, distant M subdwarfs using HST (Gould et al. 1998) predict ~ 2.5 times fewer stars at $M_V = 11$ than are found locally by Dahn et al. (1995). Dahn et al. (1995) base their study upon a sample of the local high proper motion stars in the LHS Catalog (Luyten 1979) for which they have measured accurate trigonometric parallaxes.

In this paper, we determine the luminosity function of the field Population II M subdwarfs using a new proper motion survey based upon plates taken as part of the first and second Palomar Sky Surveys. In Section 2, we discuss some general problems with the selection of halo stars. In Section 3, we describe the data used in our survey and the methods used to select a halo sample. In Section 4, we use our data to measure the M subdwarf luminosity function. In Section 5, we compare our luminosity function to other published luminosity functions and discuss its significance. In Section 6, we summarize our results. In the Appendix, we describe some stars that may be of particular interest.

2. Selection of Halo Stars — General Principles

Measurement of the Population II luminosity function is considerably more difficult than the measurement of the Population I luminosity function, for the simple reason that the Population II represents a tiny fraction of stars locally. One must either count very faint stars at large distances from the Galactic plane (Gould et al. 1998), in which case one sacrifices the ability to obtain spectroscopic data, or else determine some way to identify the local Population II stars by excluding the local $\sim 99.8\%$ of stars that belong to the disk. The latter course requires an efficient method of eliminating the disk stars before time-consuming followup observations are obtained. As members of a high velocity-dispersion, low rotation population, subdwarfs tend to have high heliocentric velocities, and choosing an initial sample of proper motion stars increases the halo contribution from $\sim 0.2\%$ to $\sim 30\%$ (Schmidt 1975). Such selection criteria introduce some kinematic bias, but lead to a much more manageable sample. Nevertheless, such a sample is still dominated by old disk (Population I) and “thick disk” (Intermediate Population II, IPII)

stars³.

As recognized by Schmidt (1975) and further discussed by Bahcall & Casertano (1986, hereafter BC), even a small proportion of contamination by high velocity disk stars can lead a gross overestimate of the space density of the halo. In order to ensure a pure halo sample for his study, Schmidt imposed a restrictive velocity criterion ($v_{tan} > 250$ km/s) and then applied a correction to account for halo stars with smaller velocities. BC used Monte Carlo simulations to estimate a correction factor of 3.03 for a cutoff velocity of 220 km s⁻¹ (this correction is dependent on the kinematics assumed for the underlying population). Most recently, this technique has been used to derive a halo luminosity function from the LHS catalog stars with $0.8''\text{yr}^{-1} \leq \mu \leq 2.50''\text{yr}^{-1}$ and $11.0 < m_r < 18.1$ (Dahn et al. 1995).

If trigonometric parallaxes are available for the target stars, then the distances and tangential velocities are estimated easily and the appropriate kinematic criteria can be applied. This is the case for the Schmidt (1975) sample and the Dahn et al. (1995) samples. Measurement of a useful trigonometric parallax requires years of observing — and the target must be relatively close ($d \lesssim 100$ pc). Expansion of the sample to cover a larger space volume requires a less direct method of distance estimation. Photometric parallaxes provide that method, with the calibrating color-absolute magnitude relations provided by subdwarfs with high quality trigonometric parallaxes.

The efficiency of the initial selection of halo candidates can be increased by use of the “reduced proper motion”, H , first used by Luyten (1939). It is defined as

$$H = m + 5 \log \mu + 5 = M + 5 \log \frac{v_{tan}}{4.74} \quad (1)$$

where m is the apparent magnitude and M is the absolute magnitude. Note that H is distance independent and determined entirely by observables. If we assume a color-magnitude relationship, we can plot constant tangential velocity contours on the data. Figure 1 illustrates the concept, where data are plotted for 2111 M dwarfs within ~ 30 parsecs of the Sun (Reid et al. 1995; Hawley et al. 1996). (Note that the increasing proper motion bias for redder stars in the Gliese & Jahreiss 1991 nearby star catalog is clearly evident.) The lines illustrate where a disk population with halo-like velocities will lie, and how halo stars will be even more easily distinguished in the diagram.

As subluminous stars in the (M_I , (R-I)) and (M_I , (V-I)) planes, halo stars have systematically larger H than disk dwarfs at a given color, mimicking the effects of increasing v_{tan} . In contrast, the coolest metal-poor subdwarfs are superluminous in the (M_V , (B-V)) plane (Gizis 1997), and a cutoff in the (H_V , (B-V)) diagram tends to discriminate against lower-abundance stars. We

³The term Intermediate Population II, used instead of “thick disk” or “extended disk,” should not be confused with the Population II halo. Considerable evidence exists that the two populations are kinematically and chemically discrete (Majewski 1993).

have therefore defined our sample of candidate halo subdwarfs as those stars with reduced proper motion, H_I , which exceed the value predicted for *disk* dwarfs with $v_{tan} = 220 \text{ km s}^{-1}$ and of the appropriate (V-I) or (R-I) color. Since the halo stars are subluminous, this selection corresponds to a cutoff velocity that is a function of metallicity - an effect which is taken into account in the subsequent analysis.

3. Selection of Halo Stars — Data and Method

We utilized the techniques described above to define our sample. Proper motion stars were identified using the first and second epoch 48-inch Schmidt photographic plates, as described in (Section 3.1). An initial cut of the sample was made to select large tangential velocity stars (Section 3.2). We then obtained spectra of each candidate halo star to estimate its metallicity and radial velocity (Section 3.3).

3.1. Proper Motions

Table 1 lists the fields analyzed in the current survey. In each, the effective area is ~ 25 square degrees, with most having plate material spanning a baseline of at least 40 years. In each case, the first epoch plates were taken with the 48-in. Oschin Telescope as part of the first Palomar Observatory Sky Survey (hereafter POSSI). For the most part, the second epoch plates were taken in the 1980s by either the 48-in. Oschin Telescope (in the course of the Palomar Observatory Second Sky Survey, POSSII) or by the U.K. Schmidt Telescope (UKST). These second epoch plates were used by Tinney, Reid, & Mould (1993, hereafter TRM) in their determination of the disk luminosity function. All of the POSSI plates were scanned by the APM facility at the Institute of Astronomy, Cambridge, while the POSSII/UKST plates were scanned by COSMOS at the Royal Observatory, Edinburgh. One additional field, centered near the North Galactic Pole, was included. As described by Reid (1990), the second epoch plates for this field were taken at Palomar in 1976, and all plate material was scanned by COSMOS. Each of these scans yields positions (both pixel x,y positions on the plate and right ascension, declination positions on the sky), magnitudes, and morphological classification as stars, galaxies, “merged stars” or noise. All objects classified as noise were excluded from further analysis.

As a preliminary to identifying proper motion stars, all objects (stars and galaxies) identified in the scans of the plates taken at the same epoch must be matched. In the case of the first epoch POSSI data, this is straightforward, since the O and E plates (corresponding roughly to photometric B and R observations) were taken on the same night. Thus there is no real motion between the time of the observations and the plate scans can be matched by demanding positional coincidence to a high level of precision. For our second epoch TRM data, the IIIaF (photometric R) and IV-N (photometric I) plates were not observed on the same night. TRM paired the objects

identified on their scans using a 3 arcsec box. Since the TRM plates were taken ~ 3 years apart, this procedure loses the highest ($\mu \gtrsim 1$ arcsec yr^{-1}) proper motion stars. In our survey, this is not a concern because the 40 year separation between the first and second epoch, with no plates at intermediate epochs, prevents our identifying reliably stars with high proper motion due to the large number of possible pairings. The effective upper limit for our survey is $\mu=0.375$ arcsec yr^{-1} , and that limit is taken into account in our luminosity function analysis.

We should note that the TRM detections are restricted to the region within 3 degrees of the plate center in order to avoid the vignetted regions near the edge of the plates, and that the COSMOS scans did not cover the entire plate. The appropriate area of the survey is given in Table 1. Moreover, the the POSSI field centers do not correspond to the POSSII/UKST field centers. Thus, between one and four POSSI plates are paired with the TRM fields, as listed in Table 1.

The identification of the proper motion stars was made as follows. First, an initial pairing of objects within a 3 arcsecond box ($\Delta < 3''$) was made. In each field, the surface density of celestial objects is sufficiently low that matching within this radius results in an unambiguous pairing. Figure 2 illustrates the agreement between the r_P and E magnitudes for one representative pairing (POSSII Field 513 and POSSI E102). Most of the outliers evident in this plot are correct pairings of extended objects (galaxies or merged stars) — they are outliers due to differences in the definitions of magnitudes used by the two machines, as well as the different plate characteristics. For this study, we are interested only in stars, so such outliers are unimportant. Having paired the unambiguous matches, we obtain a list of unmatched objects — these objects have no counterparts within 3 arcseconds at the second epoch and are good candidates for proper motion stars. Eliminating paired objects, we find all possible matches within 15 arcsec of unmatched objects. We exclude pairings which have magnitudes inconsistent with the E – r_P relation delineated by the close matches — inconsistent being defined as a discrepancy of from >1 magnitude $r_P = 12$ to > 1.5 magnitudes at $r_P = 19$. These limits are “conservative” in the sense that some false pairings are included in order to avoid excluding true proper motion stars.

The vast majority of objects on the plate should show insignificant proper motion between the two epochs, but directly matching the right ascension and declination catalog positions leads to many (false) proper motion objects. Those spurious motions arise from systematic errors in the relative positions of the two catalogs (caused by differing plate centers, inadequacy of the plate model, plate variations, telescope differences, etc.) These systematic positional errors can be corrected by determining the transformation between the original pixel positions for the two epochs (x_1, y_1 and x_2, y_2). Both our own experience with the TRM fields and the Reid (1990) analysis showed that a polynomial solution over the entire plate works poorly, producing many false proper motion stars. Analysis over smaller regions, however, is effective. Each plate was divided into approximately one by one degree regions and the positional transformation determined using second-order two-dimensional polynomials. Only stars with $\Delta < 3''$ matches were used for the initial co-ordinate transformation, iterating twice to exclude objects with large

($> 2''$) residuals. We then used these polynomial solutions to determine the proper motions of *all* stars in the field. The stars that prove to have $\mu \geq 0.1$ arcsec yr $^{-1}$ are included in our sample of proper motion stars. The selection of the candidate halo stars is described in Section 3.2.

These proper motions are measured relative to faint stars, which have typical distances of $\sim 500 - 4000$ pc. Thus we expect the reference frame to have a small, but non-zero, mean proper motion. We derive the conversion from this relative frame to an absolute (extragalactic) frame using measurements of objects classified as galaxies. The latter are identified using the ϕ -parameter defined by Picard (1991). We take $200 < \phi < 600$ for these purposes, which provides a sample dominated by galaxies. The upper cutoff is taken to exclude the “fuzziest” galaxies — we found that these “fuzzy” galaxies have large spurious proper motions, which we attribute to a combination of the different plate material used at the different epochs, and the different scanning and centroiding techniques used at the APM and COSMOS. In Figure 3, we plot the distribution of galaxy proper motions and stellar proper motions for the fields. It is clear that the galaxies do indeed show a systematic shift with respect to the stars. Table 2 lists the median proper motions ($\Delta\mu$) derived for the galaxies, which at most amount to 5.2 mas yr $^{-1}$. We have checked these values by comparison with the projection of the solar motion and rotational lag for the IPII and halo populations. The direction of motion derived by the galaxies (i.e., the *sign* of the proper motions) agrees with the expectations. These values given in Table 2 are used to correct the relative proper motions to an absolute system:

$$\mu_{abs} = \mu_{rel} - \Delta\mu$$

We also give the observed standard deviation of the galaxian motions, with values in the range 10.6 – 17.0 mas yr $^{-1}$. These provide an estimate of the uncertainties of our proper motions, but we expect that the extended galaxies should have poorer positions, and hence less accurate proper motions, than is the case for stars.

It is evident in Table 2 that Field 831 shows the largest random errors and has absolute proper motions correction that are discrepant at the ~ 2 mas level from the adjoining fields. R. Mendez (private communication) has kindly computed model proper motions for this direction based upon the galactic structure model of Mendez & van Altena (1996). The predicted mean stellar proper motions of $(\mu_\alpha, \mu_\delta) = (3.8, -4.2)$ mas yr $^{-1}$ are in excellent agreement with our observations in Fields 829 and 832. We take this as confirmation that our simple correction technique using galaxies is adequate for our purposes. The data for Field 831 are evidently of lower astrometric quality, but the accuracy remains adequate for identifying the high proper motion stars analyzed in this study.

The NLTT catalog (Luyten 1979-1980) offers an opportunity to check both the completeness and accuracy of our measurements. As noted by many authors, identifying the NLTT stars can be difficult since some of the positions are quite poor (for example, we find a star that matches the magnitudes and proper motion of LP 621-64, but is 10 *arcminutes* east of Luyten’s position). Excluding stars which are too bright, too faint, or too blue (i.e., too faint to be seen on the POSSII

IV-N plates), we find that 122 of 137 NLTT stars are recovered, indicating a completeness of at least 89%. We find that the standard deviations of $\mu_{\alpha}^{POSS} - \mu_{\alpha}^{NLTT}$ and $\mu_{\delta}^{POSS} - \mu_{\delta}^{NLTT}$ are in the range 10 to 25 mas yr⁻¹. Luyten estimated his motions to be accurate to $\pm 15 - 25$ mas yr⁻¹. The combination of our uncertainties estimated from the galaxies and the NLTT uncertainties account for the observed scatter.

3.2. Reduced Proper Motions

Selection of halo candidates using reduced proper motion requires photometry in addition to the proper motions. We have used the photometry from the second epoch plates which provides us with R and I measurements for each star (except in the NGP field, for which we have V and I).

We adopt the photometric calibration determined by TRM using CCD measurements for each plate. Because their (“Palomar”) calibration is on a unique system, we describe it briefly here. A complete description is given by TRM. The best defined photometric system in R and I for late-type stars is the Cousins system (Cousins 1973)⁴ However, M dwarfs have strong color terms in this system because the R_C band filter extends far into the I band — as a result, the effective wavelength of the R_C filter moves redward for cooler stars, as discussed by Bessell (1986). The POSSII IIIaF emulsion plus filter combination has a sharper long-wavelength cutoff at $\lambda 6900\text{\AA}$, so the color term differs significantly from the standard Cousins system. The POSSII response is close to the Gunn r filter defined by Thuan & Gunn (1976). Therefore, TRM’s CCD calibrations of the fields used Gunn r_G and i_G filters but observed *Cousins* late-type standards. These CCD magnitudes were matched to the COSMOS photographic magnitudes. They found that no significant I color term was necessary to calibrate the observations but, as expected, a strong R color term was necessary. Thus, their photometric observations consist of an R magnitude, denoted r_P , an I magnitude, denoted i_P , and a color, denoted $(r - i)_P$, for each star. The relation between the standard Cousins color and the Palomar color is

$$(r - i)_P = 0.162 + 0.439(R - I)_C + 0.671(R - I)_C^2 - 0.36(R - I)_C^3 + 0.074(R - I)_C^4 \quad (2)$$

$$i_P = I_C \quad (3)$$

Note that TRM use the relation $i_P = I_C - 0.046$, but examination of their Figure 2 indicates that there is no offset between i_P and I_C for $(R - I)_C < 1.2$, which is the color of the halo stars in our survey. The V and I photometric calibration for the NGP field is described in Reid (1990).

The reduced proper motion diagram for Field 513 is shown in Figure 4. The solid line marks

⁴As in TRM, we use the “R” and “I” to denote generic R and I photometry on any system and indicate particular photometric systems with subscripts. Thus R-I_C is Cousins R-I, $(r - i)_P$ is TRM’s Palomar system, and $(r - i)_G$ is Gunn R-I.

the disk main sequence defined by TRM,

$$M_i = 5.56037 + 0.458615 \times (r - i)_P + 1.32084 \times (r - i)_P^2 \quad (4)$$

offset to match $v_{tan} = 220 \text{ km s}^{-1}$. Stars falling below this line (larger H_I) are identified as halo candidates for spectroscopic followup. Recently, we have pointed out that the disk main sequence shows evidence for a “kink” at spectral type M4.0 V (Gizis & Reid 1996; Reid & Gizis 1997). While this feature is not included in the TRM calibration, it occurs at $(R - I)_C \approx 1.6$, so it is not relevant to the current selection of candidate halo subdwarfs.

While our tangential velocity limit is set at 220 km s^{-1} for solar abundance stars, M subdwarfs are selected at smaller v_{tan} . The esdM enter the candidate pool for $v_{tan} > 75 \text{ km s}^{-1}$ and the brighter sdM at $v_{tan} > 125 \text{ km s}^{-1}$. The most likely contaminants, modestly metal-poor ($[m/H] \approx -0.6$) Intermediate Population II M dwarfs, lie ~ 0.5 magnitudes below the disk main sequence (Gizis 1997, Figure 7), and therefore enter at $v_{tan} > 175 \text{ km s}^{-1}$.

3.3. Spectroscopy

We obtained optical spectra of the candidate halo stars in order to determine radial velocities and metallicities. The Hale 200-in. and the Las Campanas Du Pont 100-in. telescopes were used to obtain data in the wavelength range $6100 - 7300 \text{ \AA}$ with $\sim 3 \text{ \AA}$ resolution. These parameters were chosen to correspond to the observations of nearby M dwarfs (Reid et al. 1995; Hawley et al. 1996) and M subdwarfs (Gizis 1997) that we have already published. For the 200-in. observations, we used the Double Spectrograph (Oke and Gunn 1982). In August 1995, the blue camera was set to observe $6000 - 6900 \text{ \AA}$ and the red camera was set to $6700 - 8000 \text{ \AA}$ using 600 l/mm gratings blazed at 4000 \AA and 10000 \AA respectively. In October 1995, a new red camera was installed in the double spectrograph and was used in all subsequent runs to observe the region $\lambda 6000 - 7400 \text{ \AA}$ at 1.4 \AA pix^{-1} with the 600 l/mm grating blazed at 10000 \AA . With this setup, the blue camera was used to cover $4000 - 5500 \text{ \AA}$ with a 300 l/mm grating blazed at 3990 \AA . In practice, the latter data were useful only for the bluest ($(r - i)_P < 0.6$) stars. The Du Pont observations used the modular spectrograph with a 1200 line grating blazed at 7500 \AA .

From these spectra, we determined radial velocities and spectral types. During each observing run, we observed K and M radial velocity standard stars drawn from the list of Marcy & Benitz (1989). A velocity for each candidate halo star was determined by cross-correlating with the best match standard star. Comparison of subdwarfs with known radial velocities observed during the same runs shows that the accuracy is $\pm 20 \text{ km s}^{-1}$ (Gizis 1997). Using these radial velocities, we measured TiO and CaH bandstrength indices, as defined originally by Reid et al. (1995). Each index measures the ratio of the flux (F_ν) within the absorption feature to nearby pseudo-continuum points. Table 3 lists the wavelength definitions of the features (W) and the pseudo-continuum (S1,S2) points. We have defined a spectral classification system using these indices (Gizis 1997). Stars are classified as disk stars (M V), M subdwarfs (sdM), or extreme M subdwarfs (esdM). We

have shown on the basis of model atmosphere calculations (Allard & Hauschildt 1995) that these empirical classifications correspond to $[m/H] \approx -0.5$, $[m/H] \approx -1.2 \pm 0.3$, and $[m/H] \approx -2.0 \pm 0.5$ (where $[m/H] \approx [Fe/H]$; Gizis & Reid 1997). Each halo candidate has been classified using this system.

4. The Luminosity Function

In this section, we calculate the I-band luminosity function from the data described in Section 3. The luminosity function, $\Phi(M_I)$, is defined as the number of stars per cubic parsec per magnitude in a bin centered at M_I . We use Schmidt’s (1968) $1/V_{max}$ technique to estimate $\Phi(M_I)$

$$\Phi_{obs} = \sum \frac{1}{V_{max}} \quad (5)$$

$$V_{max} = \frac{\Omega}{3} (d_{max}^3 - d_{min}^3) \quad (6)$$

Where Ω is the solid angle on the sky of the survey, d_{max} is the maximum distance that a given star could have been detected in this survey, and V_{max} is the corresponding volume. A minimum distance, D_{min} , also appears to account for the distance at which the star would have evaded detection due to the upper proper motion limit of $\mu_{max} = 0.375'' \text{ yr}^{-1}$. The maximum distance may be limited by either the lower proper motion limit ($\mu_{min} = 0.100'' \text{ yr}^{-1}$) or the limiting magnitudes (R_0, I_0), hence for a star, distance d , magnitudes (R, I),

$$d_{max} = d \times \text{Min} \left(\frac{\mu}{\mu_{min}}; \text{dex}[0.2(R_0 - R)]; \text{dex}[0.2(I_0 - I)] \right) \quad (7)$$

We estimate the associated error by assuming that each star contributes an uncertainty of $1/V_{max}$ (Felton 1976). Then

$$\sigma_{\Phi}^2 = \sum \frac{1}{V_{max}^2} \quad (8)$$

As noted in Section 2, we apply a tangential velocity cutoff in order to ensure a “pure” halo sample. We adopt a value of $v_{cutoff} = 200 \text{ km s}^{-1}$ in our main analysis. As a result, a correction must be applied to the apparent luminosity function in order to obtain the space of density of halo stars. Thus,

$$\Phi_{halo} = \frac{1}{\chi} \Phi_{obs} \quad (9)$$

The discovery fraction χ is a function of position on the sky and the adopted v_{cutoff} . In our case, we compute χ for each field in the survey. This procedure is described in Section 4.2.

A check on the completeness of the survey can be made by considering

$$\left\langle \frac{V}{V_{max}} \right\rangle = \left\langle \left(\frac{d}{d_{max}} \right)^3 \right\rangle \quad (10)$$

which considers the ratio of the volume V corresponding to the star's actual distance d to V_{max} . In the case of a spatially uniform sample, such as the halo over the volume probed by this survey, we expect $\langle \frac{V}{V_{max}} \rangle = 0.5$. We find that eight of our nine fields are within 1σ of 0.5 for sdM/esdM with $v_{tan} > 200$ km s $^{-1}$, and conclude that, as a whole, the survey is complete statistically.

4.1. Adopted Color-Magnitude Relations

We use the photometry and parallax data compiled by Gizzis (1997) to determine color-magnitude relations appropriate for each spectral class of star (M V; sdM; esdM). There are many sdM and esdM with accurate distance determinations available, mainly due to the efforts of the USNO CCD parallax program (Monet et al. 1992), which allows us to determine the following relations:

$$M_I^{sdM} = 4.24 + 2.40 \times (V - I) \quad (11)$$

$$M_I^{esdM} = 4.58 + 2.92 \times (V - I) \quad (12)$$

These relations are valid for $(V - I) \geq 1.6$. Our survey is aimed at the fainter, redder M subdwarfs, but for comparisons to other surveys of higher mass stars it is useful to have an estimate of the main sequence for the bluer subdwarfs. For these stars, the above linear relations are no longer appropriate, due to an inflection in the main sequence at $V - I \sim 1.5$ (c.f., D'Antona & Mazzitelli 1996; Baraffe et al. 1997). Unfortunately, there are few parallax K subdwarfs and fewer with red (RI) photometry. The Hipparcos mission, however, has determined parallaxes for many G subdwarfs. We therefore fit a linear relation to the Hipparcos G subdwarfs supplemented by the available K subdwarfs from the Fourth Edition of the Yale Parallax Catalog (van Altena et al. 1996). In this region, models predict that for $[m/H] \lesssim -1$ the absolute magnitudes are relatively insensitive to metallicity (Baraffe et al. 1997). We select only stars with $v_{tan} > 220$ km s $^{-1}$ to ensure a halo sample. The data are shown in Figure 5. There are 29 subdwarfs with $\frac{\sigma_\pi}{\pi_t} < 0.2$, $5 \leq M_V < 10$, and $0.5 < V - I < 1.4$. We find

$$M_I^{esdG/sdG} = 2.99 + 3.16 \times (V - I) \quad (13)$$

This slope is consistent with the slope measured in globular clusters by Santiago et al. (1996).

The above relations can only be used for the NGP field, where we have V and I photometry. Unfortunately most sdM and esdM lack R photometry, while we have only R and I data for the remaining fields in our survey. Hence we have determined the relationship between $(V - I)_C$ and $(r - i)_P$ using Equation 2 and Bessell's (1990) VRI $_C$ photometry of nearby stars. We find:

$$\begin{aligned} (r - i)_P = & 0.1477 + 0.4520(V - I)_C - 0.3932(V - I)_C^2 + \\ & 0.3606(V - I)_C^3 - 0.1020(V - I)_C^4 + 0.009343(V - I)_C^5 \end{aligned} \quad (14)$$

Applying this transformation to the $(V - I)_C$ color of each parallax star, we find that

$$M_I^{sdM} = 5.37 + 3.53 \times (r - i)_P \quad (15)$$

$$M_I^{esdM} = 5.96 + 4.29 \times (r - i)_P \quad (16)$$

Relations 15 and 16 are valid for $(r - i)_P \geq 0.77$. It is possible that the R-I,V-I transformation for the extreme M subdwarfs is not the same as that for disk M dwarfs. While the currently available photometry (summarized in Gizis 1997) is unable to resolve this issue, we have obtained spectrophotometry (Gizis 1998a) which indicates that there is no significant color term for the sdM stars or the earliest (esdK7; esdM0.0) extreme subdwarfs.

For the G subdwarfs, we transform Equation 13 and obtain:

$$M_I^{esd/sdG} = 1.98 + 8.26 \times (r - i)_P \quad (17)$$

Equation 17 applies for $0.31 < (r - i)_P < 0.66$.

4.2. Kinematic Corrections

The luminosity function computed using the techniques described above, although correct in shape, represents only the fraction of the halo that has $v_{tan} \geq v_{cutoff}$ km s $^{-1}$. Given a kinematic model of the halo, we can calculate the discovery fraction (χ) for each field using Monte Carlo simulations. BC have shown that variations of ± 5 km s $^{-1}$ in the kinematic parameters ($\langle \langle V \rangle \rangle, \sigma_U, \sigma_V, \sigma_W$) imply variations of less than 4% in χ ; sadly, published data for halo stars span a much larger range of kinematics. We therefore compare the observed kinematics of our survey stars to the predictions of representative halo models.

Analyses of local ($d < 1$ kpc) halo stars generally derive mild prograde rotation (e.g., 37 ± 10 km s $^{-1}$, Norris 1986), although recent studies based on more distant (> 5 kpc) halo stars have found evidence for a retrograde rotating halo (see the review of Majewski 1993). We compare our data to the models of Bahcall & Casertano (1986, BC), Norris (1986, N), Casertano et al. (1990, CRB), Layden et al. (1996, L), and Beers & Sommer-Larson (1995, BSL). The last is of considerable interest as it features a retrograde rotating halo.

For each of these models, we generated a Monte Carlo simulation of our survey with ~ 5000 detected stars. The halo velocities are represented by Gaussian distributions in U,V, and W.⁵ In Table 5, we compare the predictions of the U,V, and W velocity distributions of the models to the actual data for the 35 metal-poor stars with $M_I > 8.5$. We emphasize that these are the predicted velocity characteristics of the kinematically-biased observed sample, not the true halo kinematics. We also give the probability that the observed data and the model simulations are drawn from the same distributions, as determined by Kolmogorov-Smirnov tests. The comparison is most sensitive to the observed V velocities, which are most important in determining χ . It is clear that all

⁵We use the standard notation of (U,V,W) for the space velocity components, in which U represents the motion towards the Galactic center ($l = 0, b = 0$), V represents motion in the direction of Galactic rotation, and W represents motion perpendicular to the Galactic plane.

the published models agree fairly well with the observed U and W velocity distribution, although the N model is significantly poorer for U, due to its smaller velocity dispersion ($\sigma_U = 131 \text{ km s}^{-1}$). The V velocities favor prograde halos, with the BC model ($v_{rot} = 66 \text{ km s}^{-1}$) yielding too small a mean V velocity and the N model ($v_{rot} = 37 \text{ km s}^{-1}$) yielding too large a mean velocity. The BSL model’s retrograde halo is much less likely than the prograde models. Of the published models, the Layden et al. model gives the highest probability when all three velocity components are considered.

Guided by the comparison above, we have constructed a composite kinematic model, taking the parameters derived by Norris as a starting point and increasing both σ_U to match other studies, and the halo rotation to a value midway between BC and N. The resulting parameters are $(v_{rot}, \sigma_U, \sigma_V, \sigma_W) = (+50, 140, 106, 85)$ in km s^{-1} and we refer to this as our model A. These changes are within 1.5σ of Norris’s estimated uncertainties. The values of $1/\chi$ for the BC and N models lie within $\pm 7\%$ of the composite values, which are listed in Table 4. Values of $1/\chi$ based on the Layden et al. halo model are on average 20% smaller.

We have also calculated models including the IPII (BSL, CRB). Only one in ~ 400 IPII stars will enter our $v_{tan} > 220 \text{ km s}^{-1}$ sample (although we caution that this number depends upon the assumption of Gaussian kinematics). Since the IPII consists of approximately 2 – 5% of stars locally, it will contribute less than 10% of our observed halo sample and thus will not bias significantly our measurements. This can also be seen in Table 1 of BC, where it is shown that the kinematic properties of stars in Eggen’s (1979a, 1980) proper motion catalog with $v_{tan} \geq 200$, $v_{tan} \geq 220$ and $v_{tan} \geq 250 \text{ km s}^{-1}$ are indistinguishable. We expect that the IPII contribution is much less than this, since direct spectroscopic observation shows that most IPII M dwarfs both locally (nearby stars with $100 \leq v_{tan} \leq 220 \text{ km s}^{-1}$, Gizis 1997) and at height of a few kiloparsecs (Reid et al. 1997) are not classified as sdM or esdM. We reject all spectroscopic M V stars from our sample, and therefore we expect negligible IPII contamination.

For each field, we calculate the luminosity function using the Equations 5 to 7 using only stars with $v_{tan} \geq 200 \text{ km s}^{-1}$. We combine data for all fields to derive our best estimate luminosity function, calculated for 0.5 magnitude bins, which is listed in Table 6.

These conservative selection criteria ensure a pure Population II halo sample but suffers from the uncertainty of the kinematic correction. Since we have obtained spectroscopy for all of our reduced proper motion selected stars, we have information on the actual space density of metal-poor very-low-mass stars with lower velocities ($v_{tan} > 100 \text{ km s}^{-1}$ for esdM; $v_{tan} > 125 \text{ km s}^{-1}$ for sdM). We have therefore computed the space density of sdM and esdM separately, using the appropriate velocity cutoff for each metallicity class. The completeness corrections, $\frac{1}{\chi}$, for these velocity cutoffs are only $\sim 10 – 20\%$, since virtually all halo stars have $v_{tan} > 125 \text{ km/s}$. The resulting luminosity functions for the sdM and esdM are listed in Table 7. This luminosity function is remarkably consistent with that estimated from the corrected “pure” halo sample. The normalizations differ by no more than 20% from that predicted by our composite model. We

discuss these low- v_{tan} samples in more detail in Section 5.

5. Discussion

Our measurement of the Population II luminosity function is aimed at only the limited range in luminosity corresponding to the fainter M subdwarfs. Nonetheless, these results offer a means of resolving the difference, noted in the Section 1, between Gould et al.’s HST starcount analysis at $\gtrsim 5$ kpc and Dahn et al.’s local trigonometric parallax sample. Before discussing that issue, we consider whether our results can be combined with previous measurements of the bright end of the halo luminosity function. Since previous studies of the halo luminosity function have presented $\Phi(M_V)$ for all metallicities combined, we have transformed our data using the relation

$$\Phi(M_V) = \Phi(M_I) \frac{dM_I}{dM_V} \quad (18)$$

and the color-magnitude relations given in Section 4.1. The results for the combined sdM and esdM luminosity function is plotted in Figure 6. The other luminosity functions shown are the local trigonometric parallax samples of Schmidt (1975) and Dahn et al., the local photometric parallax sample of Bahcall & Casertano (1986), and the Gould et al. HST starcount analysis. We have not plotted Dawson’s (1986) statistical analysis of the LHS stars, since it is superceded by Dahn et al.’s calculations, which have the advantage of improved data for individual stars. Schmidt’s results have been updated using literature V-band photometry, but there are only 0-2 stars per bin, except for the last two bins which have five stars apiece. It should also be noted that, except for the HST data, these estimates of $\Phi(M_V)$ are based on kinematically-selected samples. Dahn et al.’s v_{tan} correction factors, χ , agree to within 5% with the values predicted by our model A, and we have also used that model to adjust Schmidt’s data. The Bahcall & Casertano $\Phi(M_V)$ plotted is derived using their published correction factors. Adopting χ appropriate to model A reduces the inferred space densities by 15%, increasing the discrepancy with respect to the other studies (including our own results).

It is obvious from Figure 6 that there are potential problems involved in combining data from the several investigations to derive a halo luminosity function spanning the full range in absolute magnitude. Of the surveys which include brighter stars near the turnoff, Schmidt’s luminosity function (as noted originally by Schmidt!) has too few stars to measure reliably the shape of the luminosity function. The BC dataset has sufficient stars, but there is a clear, systematic offset of almost a factor of two between their derived space densities and Dahn et al.’s results. Bahcall & Casertano’s analysis is based on Eggen’s (1979a, 1980) survey of southern ($\delta < 30^\circ$) stars with $\mu > 0''.7 \text{ yr}^{-1}$ and $V < 15$, but a comparison of both the relative numbers and V/V_{max} distributions of such stars shows no evidence for any significant increase in incompleteness at southern declinations. On the other hand, the color-magnitude relation (from Eggen, 1979b) which BC use to estimate distances is a poor description of the lower Pop. II main sequence ($M_V \gtrsim 9 - 10$), and therefore that portion of $\Phi(M_V)$ should probably be excluded. The calibration

is likely to be more reliable for the more luminous stars, since the main sequence is consistent with the Hipparcos data in Figure 5 for the G subdwarfs.

One notable aspect of the Eggen/BC sample is that it may be incomplete in the Galactic Plane, since it is difficult to identify proper motion stars against the dense stellar background. We have simulated halo samples using the BC, A, and L models for both “all-sky” ($\delta < 30$) and “non-plane” ($\delta < 30$ and $|b| > 20$) selection. The kinematic correction factors ($1/\chi$ for $v_{tan} > 220$ km s $^{-1}$) for the “non-plane” samples are greater than the “all-sky” samples by between 8% and 12% depending on the model. However, our analysis of the Eggen (1979a, 1980) data shows that the derived halo space density for stars with $|b| > 20$ is actually $\sim 40\%$ higher than that derived for the entire Eggen sample. This suggests that the BC luminosity function is underestimated by $\sim 30\%$ due to incompleteness in the Galactic Plane. This would account for about a third of the discrepancy evident in Figure 6.

Naively combining the higher-luminosity stars from BC with Dahn et al. and our own results for fainter stars suggests a rather steep luminosity function. Globular clusters provide a potential means of testing this result. Figure 7 compares $\Phi(M_I)$ from the field against results for two of the better-studied clusters, using data from Piotto et al. (1997) adjusted to be consistent with the new distances derived by Reid (1997) on the basis of main-sequence fitting. That comparison suggests that the BC results may underestimate the space densities of stars with $6.5 < M_I < 8$, consistent with the offset between the BC and Dahn et al results plotted in Figure 6. It should of course be noted that the field and cluster luminosity functions may differ – the present-day luminosity (mass) function of globular clusters could be affected by dynamical evolution, or alternatively the initial mass function of field and cluster stars could be different. Extension of the Dahn et al. sample to brighter absolute magnitudes (e.g., expanding the Schmidt sample) should provide the most effective means of confirming the shape of the field luminosity function. The Dahn et al. luminosity function, transformed via Equation 12 is also plotted, but the transformation is uncertain since we have assumed all stars to be esdM, which is not the case — and in any case, this preliminary Dahn et al. luminosity function represents a range of metallicities, so it may not be fair to compare it to the globular clusters. Nevertheless it is clear that the Dahn et al. luminosity function peaks at a fainter absolute magnitude than the globular clusters.

As noted above, Figure 6 suggests that the Gould et al (1998) HST analysis underestimates the local density of late-type halo subdwarfs by a factor of four. To underscore that point, Figure 8 plots our luminosity function against a $\Phi(M_I)$ representation of the HST data that was computed by Gould (private comm.) using the same data and techniques used to derive the M_V luminosity function of Gould et al. (1998). While our study is limited to a restricted range of luminosity, the space densities, derived from a completely independent sample of nearby subdwarfs, are clearly strongly supportive of the LHS-star analysis. A possible resolution of the discrepancy between the distant-halo and local-halo analyses may lie in the composite nature of the galactic halo. Sommer-Larsen & Zhen (1990) estimate that at least 40 percent of the local subdwarfs reside in a highly-flattened component, which would essentially be absent from the HST dataset. Taken

in isolation, this additional component can account only partially for the factor of four offset in the derived densities. However, its presence underlines the substantial extrapolation involved in transforming the observed number density at large distances from the Plane to a local halo subdwarf density. An additional contribution could be due to the choice of local calibrating subdwarfs for the Gould et al. analysis, which may be biased towards higher metallicities. This would lead to overestimated M_V and distance, and hence an underestimate of the space density. For a discussion of possible systematic errors, see Gould et al.’s discussion.

The kinematics of the very-low-mass halo stars are consistent with those found for higher mass metal-poor stars. The strongest conclusion is that prograde rotating halos are favored. If the expanded halo sample that includes lower tangential velocity stars is included, then kinematics like those of model A is favored over Layden et al.’s RR Lyrae kinematics, since the expanded luminosity function is more consistent with the model A corrected pure halo sample (Tables 6 and 7). There *may* be an excess of sdM at low velocities over the halo model A predictions. Since metallicities of $[m/H] \approx -1.2 \pm 0.3$ are expected to have some IPII contribution, this is not too surprising. If the two best determined bins are used, then the excess is only 19%. Chiba & Yoshii (1998) find an excess of $\sim 20\%$ in the range $-1.4 < [Fe/H] \leq -1.0$ based upon Hipparcos data for red giant and RR Lyrae stars, in excellent agreement with our results.

The mass function can be estimated using the observed luminosity function and a mass-luminosity relation as follows:

$$\Psi(M) = \Phi(M_I) \frac{dM_I}{dM} \quad (19)$$

This is often parameterized as a power-law with the form

$$\Psi(M) = \frac{dN}{dM} \propto M^{-\alpha} \quad (20)$$

Since there are no direct determinations of mass for any sdM or esdM stars, we must rely upon theoretical mass-luminosity relations. These must be viewed with caution – for example, Reid & Gizis (1997) have shown that, in the case of the Baraffe et al solar-abundance models, the slope deduced from nearby-star data for the disk mass function depends on the passband used in the analysis. Our data do not provide sufficient range in M_I to estimate the mass function reliably, even given a good mass-luminosity relationship, but it does allow us to estimate the relative numbers of sdM and esdM stars at a mass of $0.2M_\odot$. We transform the observed pure halo M_I luminosity functions into mass functions using the Baraffe et al. (1997) models. We adopt the $[m/H] = -1.0$ and $[m/H] = -1.5$ interior models for the sdM and esdM respectively, and fit a power-law to the mass function in order to obtain the best estimate of the numbers. The ratio of sdM to esdM at $0.225M_\odot$ is 0.38. In comparison, we obtain a ratio of 0.36 if we adopt the Alexander et al. (1997) models, and 0.60 for the D’Antona & Mazzitelli (1996) tracks — but the latter match the observed $V - I, M_I$ main sequence poorly. These results are consistent with the Carney et al. (1994) distribution of metallicities for higher mass stars (mainly G subdwarfs) — 41% of their stars in a pure ($V < -220$ km s $^{-1}$) halo sample have $[m/H] > -1.5$. Thus, the

metallicity distribution for the very-low-mass stars of the halo ($M \approx 0.2M_{\odot}$) is apparently the same as that of stars on the upper main sequence ($M \approx 0.7M_{\odot}$). Barring a cosmic conspiracy of offsetting parameters, the most reasonable explanation is that the mass function in the halo is independent of metallicity. Although our data is inadequate to constrain the mass function well, we note that the best-fit parameters are $\alpha \approx 0.5 \pm 1.6$ for the esdM and 1.3 ± 0.9 for the sdM. These compare with a power-law index of $\alpha = 1.05 \pm 0.15$ for disk stars in the mass range $1.0 > \frac{M}{M_{\odot}} > 0.1$ (Reid & Gizis 1997).

The consistency of the metallicity distribution and kinematics of the low-mass stars (sdM and esdM) is not surprising, but nevertheless important. Studies of the halo, whether using evolved stars such as RR Lyrae or red giants, or main sequence stars (F,G subdwarfs), assume that the properties of stars in the narrow mass range from just below the turnoff to the tip of the asymptotic giant branch ($0.6 - 0.8M_{\odot}$), are representative of the halo population as a whole. Our results verify one aspect of this assumption for stars near the bottom of the halo main sequence.

6. Summary

We have derived a new estimate of the space density of very low mass metal-poor stars. Comparisons with other surveys shows that we are in agreement with the Dahn et al. (1995) survey based upon trigonometric parallaxes of LHS catalog stars. This implies that the local space density of metal-poor stars is higher than that predicted by HST observations of more distant stars.

Our work provides measurements of the kinematics and metallicity distribution of very-low-mass stars. These measurements are consistent with those from studies of higher-mass stars in the halo. We find that the esdM are 2.5 times as common as sdM at $\sim 0.2M_{\odot}$. This is consistent with the relative numbers of metal-poor ($[m/H] \leq -1.5$) and metal-rich ($[m/H] > -1.5$) G subdwarfs found by Carney et al. (1994). Note that the two metallicity scales are comparable because Gizis & Reid (1997) have found agreement between the Carney et al. metallicities of FGK subdwarf primaries with metallicities based upon G97. The agreement of the metallicity distribution at both low and high mass implies that the mass function is not a strong function of metallicity for ($M \lesssim 0.7M_{\odot}$) halo stars. This result is supported by the general similarity of the mass functions derived for the two metallicity bins considered; however, those mass functions depend upon uncertain model mass-luminosity transformations.

We thank Chris Tinney and Mike Irwin for assistance with the plate scans and the staff of Palomar Observatory for their capable support. We also thank M. Schmidt for useful conversations and A. Gould for providing the I-band HST luminosity function. J.E.G. is grateful for partial support through Greenstein and Kingsley Fellowships as well as NASA grants GO-05353.01-93A, GO-05913.01-94A, and GO-06344.01-95A. This work is based partly

on photographic plates obtained at the Palomar Observatory 48-inch Oschin Telescope for the Second Palomar Observatory Sky Survey which was funded by the Eastman Kodak Company, the National Geographic Society, the Samuel Oschin Foundation, the Alfred Sloan Foundation, the National Science Foundation grants AST84-08225, AST87-19465, AST90-23115 and AST93-18984, and the National Aeronautics and Space Administration grants NGL 05002140 and NAGW 1710. This research has made use of the Simbad database, operated at CDS, Strasbourg, France.

A. Stars of Particular Interest

Most of our subdwarfs lie at distances of greater than 200 parsecs, and therefore are more difficult to study than LHS Catalog subdwarfs. Three of our stars, however, are close enough that additional observations may be profitable. All were previously identified by Luyten (1979-1980). The positions (B1950, at the epoch given in Table 1) and other data for these stars are given in Table 8. Spectra of the subdwarfs LP 622-7 and LP 382-40 are plotted in Figure 9. LP 622-7 has a proper motion too large to be included in our complete sample, and was observed at the Palomar 60-in. in June 1995. The radial velocity may be unreliable due to a problem with the calibrating arc lamp exposure.

LP 589-7 is one of the coolest subdwarfs known. Its spectral indices are $\text{TiO5}=0.68$, $\text{CaH1}=0.48$, $\text{CaH2}=0.27$, and $\text{CaH3}=0.50$. In Figure 10, we show that this star is extremely similar to the esdM5.0 (Gizis 1997) star LHS 3061 ($M_I=11.65$, Monet et al. 1992). The conspicuous TiO absorption at 7050\AA distinguishes both these stars and the slightly cooler LHS 1742a ($M_I=11.69$, esdM5.5) from the other two very cool extreme subdwarfs LHS 205a ($M_I=11.65$, esdM5.0) and LHS 1826 (M_I unknown, esdM6.0; Gizis & Reid 1997). LP 589-7 is just as close as LHS 1742a, so it is an excellent candidate for a trigonometric parallax.

There is a hint of $H\alpha$ emission in our spectrum of LP 589-7. The feature, which may not be real but lies at the correct wavelength, has an equivalent width of $\sim 1.2\text{\AA}$. Two sdM systems (LHS 482 and LHS 2497) are known to show emission due to close companions (Gizis 1998b). Since LP 589-7 is near the hydrogen burning limit, any companion must be either a very faint, old white dwarf (as for the LHS 482 system), a nearly equal luminosity M companion (as for LHS 2497), or else a brown dwarf (if it proves to be too faint to contribute detectable light). Alternatively, LP 589-7 could be a “young” metal-poor star with an age of up to a few billion years. If an SB2, its estimated distance and tangential velocity should be increased by up to 40%. All this is speculative, however, since the $H\alpha$ feature is weak and may not be real.

REFERENCES

Alexander, D.R., Brocato, E., Cassisi, S., Castellani, V., Ciacio, F., & Degl’Innocenti, S. 1997, *A&A*, 317, 90

Allard, F., & Hauschildt, P.H. 1995, *ApJ*, 445, 433

Bahcall, J.N., & Casertano, S. 1986, *ApJ*, 308, 347 (BC)

Baraffe, I., Chabrier, G., Allard, F., & Hauschildt, P.H. 1997, *A&A*, 327, 1054

Baraffe, I., Chabrier, G., Allard, F., & Hauschildt, P.H. 1998, *A&A*, 337, 403

Beers, T.C., & Sommer-Larsen, J. 1995, *ApJS*, 96, 175

Bessell, M.S. 1986, *PASP*, 98, 1303

Carney, B.W., Latham, D.W., Laird, J.B., and Aguilar, L.A. 1994, *AJ*, 107, 2240

Casertano, S., Ratnatunga, K.U., Bahcall, J.N. 1990, *ApJ*, 357, 435

Chiba, M., & Yoshii, Y. 1998, *AJ*, 115, 168

Cool, A.M., Piotto, G., & King, I.R. 1996, *ApJ*, 468,, 655

Cousins, A.W.J. 1973, *Mem.R.A.S.*, 77, 223

Dahn, C.C., Liebert, J., Harris, H.C., & Guetter, H.H. 1995, The Bottom of the Main Sequence — And Beyond, edited by C.G. Tinney (Berlin, Springer), p.239

D'Antona, F., & Mazzitelli, I. 1996, *ApJ*, 456, 329

Dawson, P.C. 1986, *ApJ*, 311, 984

Eggen O.J. 1979a, *ApJS*, 39, 89

Eggen O.J. 1979b, *ApJS*, 230, 786

Eggen O.J. 1980, *ApJS*, 43, 457

Felton, J.E. 1976, *ApJ*, 207, 700

Gizis, J.E. 1997, *AJ*, 113, 806

Gizis, J.E. 1998a, Ph.D. Thesis, California Institute of Technology

Gizis, J.E. 1998b, *AJ*, 115, 2053

Gizis, J.E., & Reid, I.N. 1996, *AJ*, 111, 365

Gizis, J.E., & Reid, I.N. 1997, *PASP*, 109, 894

Gliese, W., & Jahreiss, H. 1991, Preliminary Version of the Third Catalog of Nearby Stars (CNS3)

Gould, A., Flynn, C., Bahcall, J.H. 1998, *ApJ*, in press

Hawley, S.L., Gizis, J.E., & Reid, I.N. 1996, AJ, 112, 2799

Layden, A.C., Hanson, R.B., Hawley, S.L., Klemola, A.R., & Hanley, C.J. 1996, AJ, 112, 2110

Luyten, W.J. 1939, Publ. Minnesota, 2, 121

Luyten, W.J. 1979, Catalogue of stars with proper motions exceeding 0".5 annually (LHS), (University of Minnesota, Minneapolis, Minnesota)

Luyten W. J., 1979-1980, New Luyten Catalogue of Stars with Proper Motions Larger than Two Tenths of an Arcsecond, (Minneapolis, University of Minnesota), computer-readable version on ADC Selected Astronomical Catalogs Vol.1 - CD-ROM

Marcy, G.W., & Benitz, K.J. 1989, ApJ, 344, 441

Majewski, S.R. 1993, ARA&A, 31, 575

Mendez, R.A., & van Altena, W.F. 1996, AJ, 112, 655

Monet, D.G., Dahn, C.C., Vrba, F.J., Harris, H.C., Pier, J.R., Luginbuhl, C.B., & Ables, H.D. 1992, AJ, 103, 638

Mould, J.R. 1996, PASP, 108, 35

Murray, S.D., & Lin, D.C. 1996, ApJ, 467, 728

Norris, J. 1986, ApJS, 61, 667

Oke, J.B., & Gunn, J.E. 1982, PASP, 94, 586

Paresce, F., De Marchi, G., & Romaniello, M. 1995, ApJ, 440, 216

Picard, A. 1991, AJ, 102, 445

Piotto, G., Cool, A.M., King, I.R. 1997, AJ, 113, 1345

Reid, N. 1990, MNRAS, 247, 70

Reid, I.N. 1997, AJ, 114, 161

Reid, I.N., Hawley, S.L., & Gizis, J.E. 1995, AJ, 110, 1838

Reid, I.N., & Gizis, J.E. 1997, AJ, 113, 2246

Reid, I.N., Gizis, J.E., Cohen, J.G., Pahre, M.A., Hogg, D.W., Cowie, L., Hu, E., & Songaila, A. 1997, PASP, 109, 539

Santiago, B.X., Gilmore, G., Elson, R.A.W. 1996, MNRAS, 281, 871

Schmidt, M. 1968, ApJ, 151, 393

Schmidt, M. 1975, ApJ, 202, 22

Sommer-Larsen, J. & Zhen, C. 1990, MNRAS, 242, 10

Stobie, R.S., Ishida, K., & Peacock, J.A. 1989, MNRAS, 238, 709

Tinney, C.G., Reid, I.N., & Mould, J.R. 1993, ApJ, 414, 254 (TRM)

Thuan, T.X., & Gunn, J.E. 1976, PASP, 88, 543

van Altena, W.F., Lee, J.T., & Hoffleit, E.D. 1995, The General Catalogue of Trigonometric
Stellae Parallaxes, Fourth Edition (Schenectady, L. Davis Press)

Zinnecker, H. 1995, The Bottom of the Main Sequence — And Beyond, edited by C.G. Tinney
(Berlin, Springer), p.257

Table 1. Survey Fields

Field	α	(B1950)	δ	Source	Epoch	Plate	Epoch
829	02	00	+00	UK/PII	1987.83	EO852	1953.78
831	02	40	+00	UK/PII	1981.92	EO1283	1954.90
						EO1453	1955.81
832	03	00	+00	UK/PII	1986.89	EO363	1951.69
						EO1453	1955.81
262	10	15	+45	POSSII	1987.34	EO672	1953.12
NGP	13	04	+29	Palomar	1976.23	EO1393	1955.29
868	15	00	+00	UK/PII	1987.30	EO1402	1955.30
						EO1613	1957.32
513	15	00	+25	POSSII	1987.34	EO102	1950.35
						EO87	1950.30
						EO1390	1955.29
						EO1092	1954.49
889	22	00	+00	POSSII	1990.55	EO1146	1954.57
890	22	20	+00	POSSII	1990.82	EO364	1951.69
						EO1146	1954.57

Table 2. Relative to Absolute Proper Motions

Field	$\Delta\mu_\alpha$	$\Delta\mu_\delta$	σ_α	σ_δ
	mas	mas	mas	mas
262	2.6	5.2	13.0	13.7
513	4.4	4.2	12.1	11.8
829	-3.7	3.8	14.9	13.9
831	-2.0	2.3	17.0	16.0
832	-4.3	3.9	13.6	12.6
868	3.2	3.3	13.6	12.6
889	-0.2	4.3	10.6	10.6
890	-0.9	3.4	11.9	11.5
NGP	5.0	3.9

Table 3. Spectroscopic Indices

Band	S1	W	S2
TiO 5	7042-7046	7126-7135	
CaH 1	6345-6355	6380-6390	6410-6420
CaH 2	7042-7046	6814-6846	
CaH 3	7042-7046	6960-6990	

Table 4. Kinematic Corrections

Field	Area (sq. deg)	m_I^{lim}	$1/\chi$
829	25.32	17.3	2.07
831	26.49	17.3	2.15
832	25.32	17.3	2.11
262	14.56	17.3	2.30
NGP	28.00	17.0	2.01
868	25.29	17.3	2.11
513	25.29	17.3	2.18
889	25.30	17.3	3.70
890	25.26	17.3	3.56

Table 5. Kinematic Comparison

	Data	BC	N	L	CRB	BSL	A
σ_U	171	171	146	179	165	155	158
Probability (U)		0.43	0.15	0.55	0.29	0.19	0.31
$\langle V \rangle$	-234	-222	-244	-240	-252	-264	-233
σ_V	76	82	82	84	73	76	85
Probability (V)		0.37	0.49	0.75	0.22	0.05	0.87
σ_W	90	77	86	97	94	105	86
Probability (W)		0.38	0.49	0.32	0.38	0.28	0.49

Table 6. Pure Halo Luminosity Functions

M_I	Φ [A]	σ_Φ [A]	Φ [L]	σ_Φ [L]	N
	10^{-5} pc $^{-3}$ Mag $^{-1}$		10^{-5} pc $^{-3}$ Mag $^{-1}$		
sdM ($v_{tan} \geq 200$ km s $^{-1}$)					
8.5	2.2	0.7	1.8	0.5	16
9.0	2.0	0.6	1.6	0.5	11
9.5	2.0	0.9	1.6	0.8	5
10.0	2.0	2.0	1.6	1.6	1
esdM ($v_{tan} \geq 200$ km s $^{-1}$)					
9.5	4.6	1.8	3.9	1.5	10
10.0	3.6	1.6	2.9	1.3	5
10.5	3.1	2.3	2.6	2.0	2

Table 7. Expanded Halo Luminosity Functions

M_I	Φ [A]	σ_Φ [A]	Φ [L]	σ_Φ [L]	N
	10^{-5} pc $^{-3}$ Mag $^{-1}$		10^{-5} pc $^{-3}$ Mag $^{-1}$		
sdM ($v_{tan} \geq 125$ km s $^{-1}$)					
8.5	2.6	0.8	2.5	0.7	20
9.0	2.4	0.8	2.2	0.7	14
9.5	4.4	1.3	4.1	1.2	12
10.0	3.1	1.6	2.9	1.5	4
10.5	3.6	3.6	3.4	3.4	1
esdM ($v_{tan} \geq 100$ km s $^{-1}$)					
9.5	6.9	1.8	6.6	1.7	20
10.0	2.5	1.0	2.4	1.0	6
10.5	4.1	2.1	3.9	2.0	4
11.0	0
11.5	0
12.0	15.	15.	15.	15.	1

Table 8. Nearby Subdwarfs

Name	α	δ	μ_α	μ_δ	i_P	$r - i_p$	M_i	d	v_{tan}	v_{rad}	Sp. Type
LP 589-7	28.72333	+1.03647	-0.12	-0.33	15.90	1.38	11.77	64	106	-65	esdM5
LP 382-40	223.53375	+23.83433	-0.28	-0.09	16.47	1.08	10.59	150	210	-230	esdM2.5/3
LP 622-7	227.18958	-1.02281	+0.20	-0.43	13.87	0.87	9.69	69	155	300	esdK7/M0

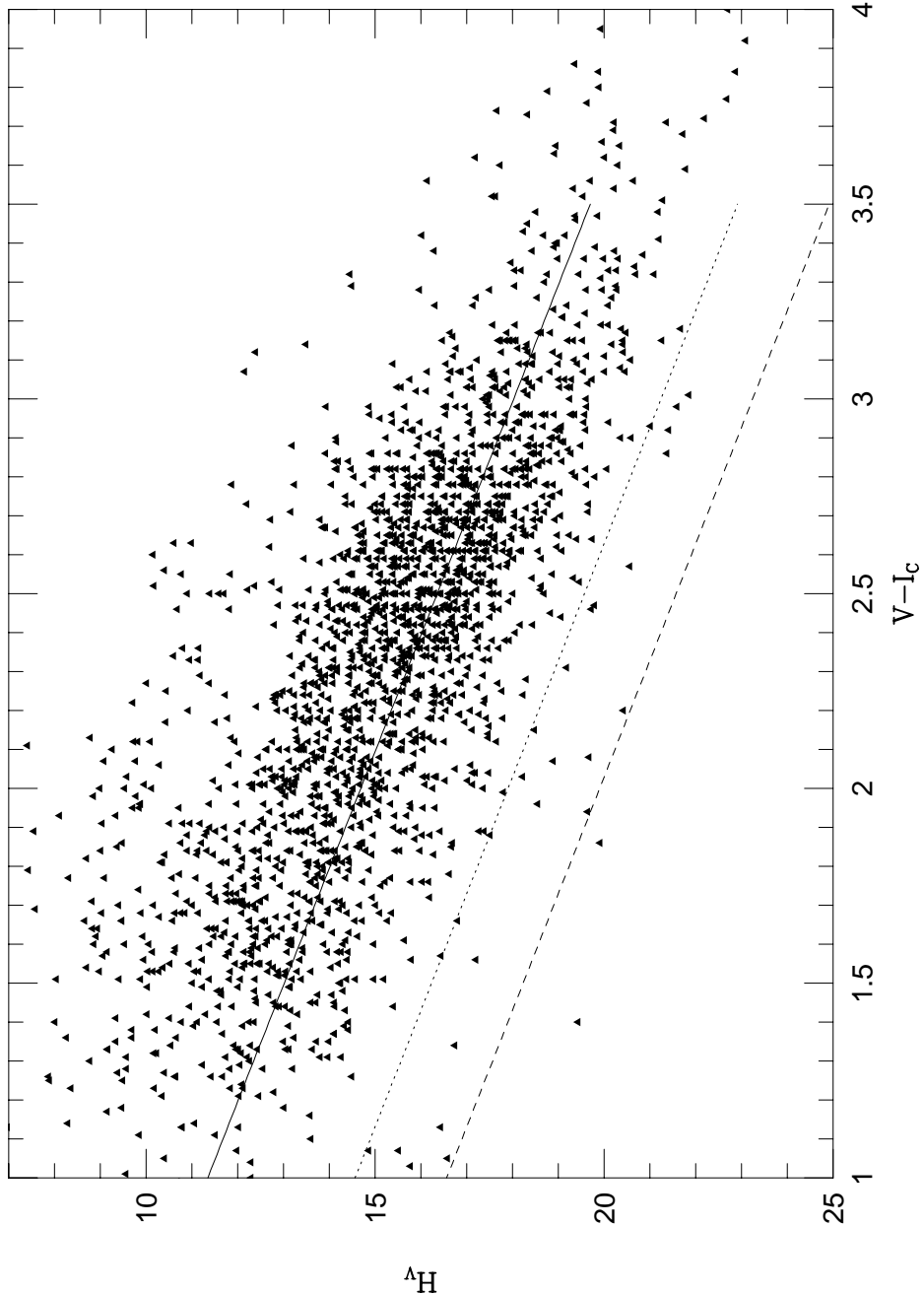


Fig. 1.— A color - reduced proper motion ($V - I, H_V$) diagram for a nearly volume limited sample of stars within 25 parsecs. The 2111 observable known nearby M dwarfs (Reid et al. 1995; Hawley et al. 1996) are plotted. For some stars, the $V - I$ photometry was estimated on the basis of their spectral type. The solid line plots a disk population using the Stobie et al. (1989) main sequence and $v_{tan} = 50 \text{ km s}^{-1}$. The dotted line plots the same main sequence with $v_{tan} = 220 \text{ km s}^{-1}$. The dashed line plots a main sequence that is two magnitudes subluminous, roughly corresponding to the ΔM_V limit of the volume limited sample. The $V - I$ limit is $H_V = 25$.

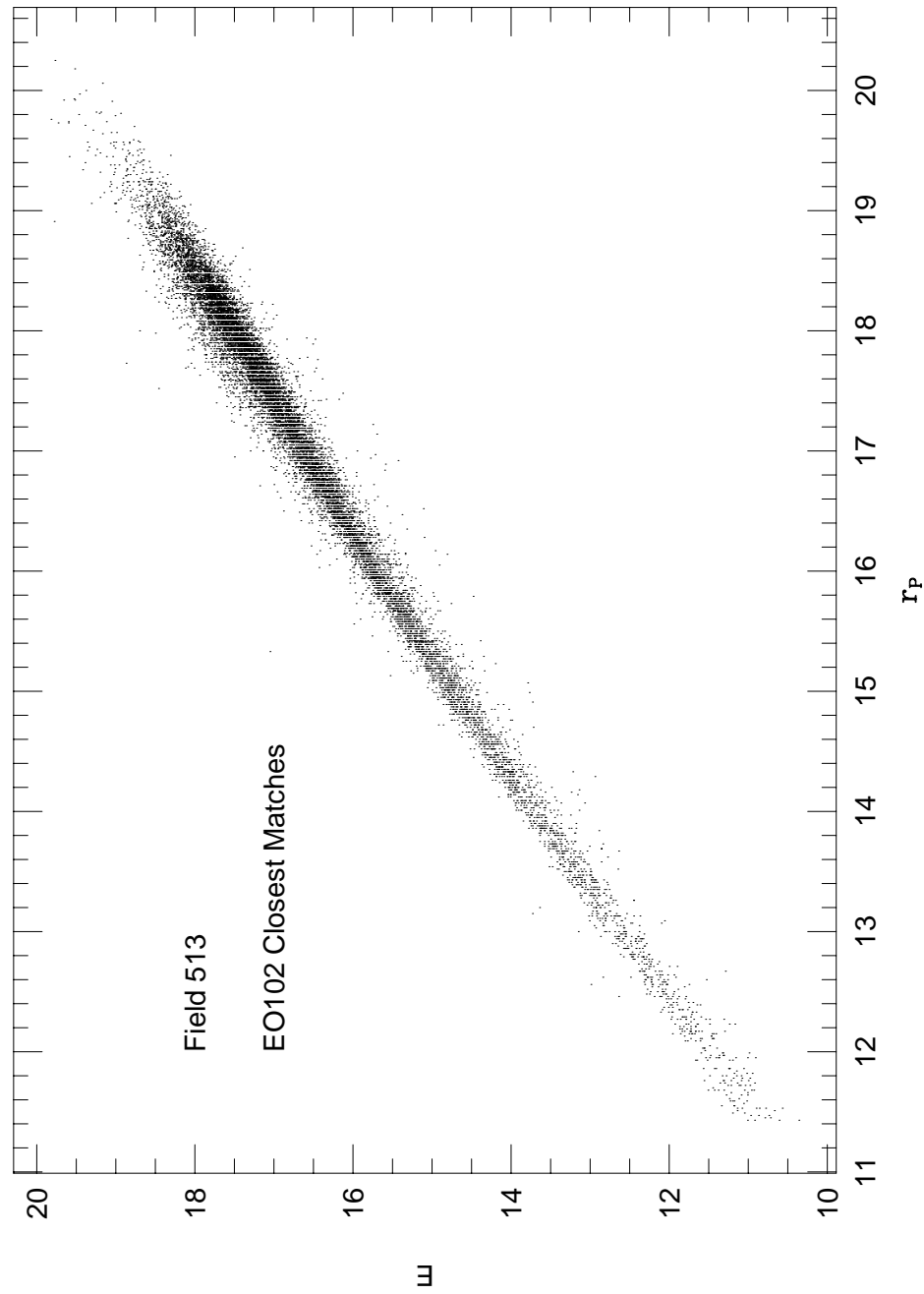
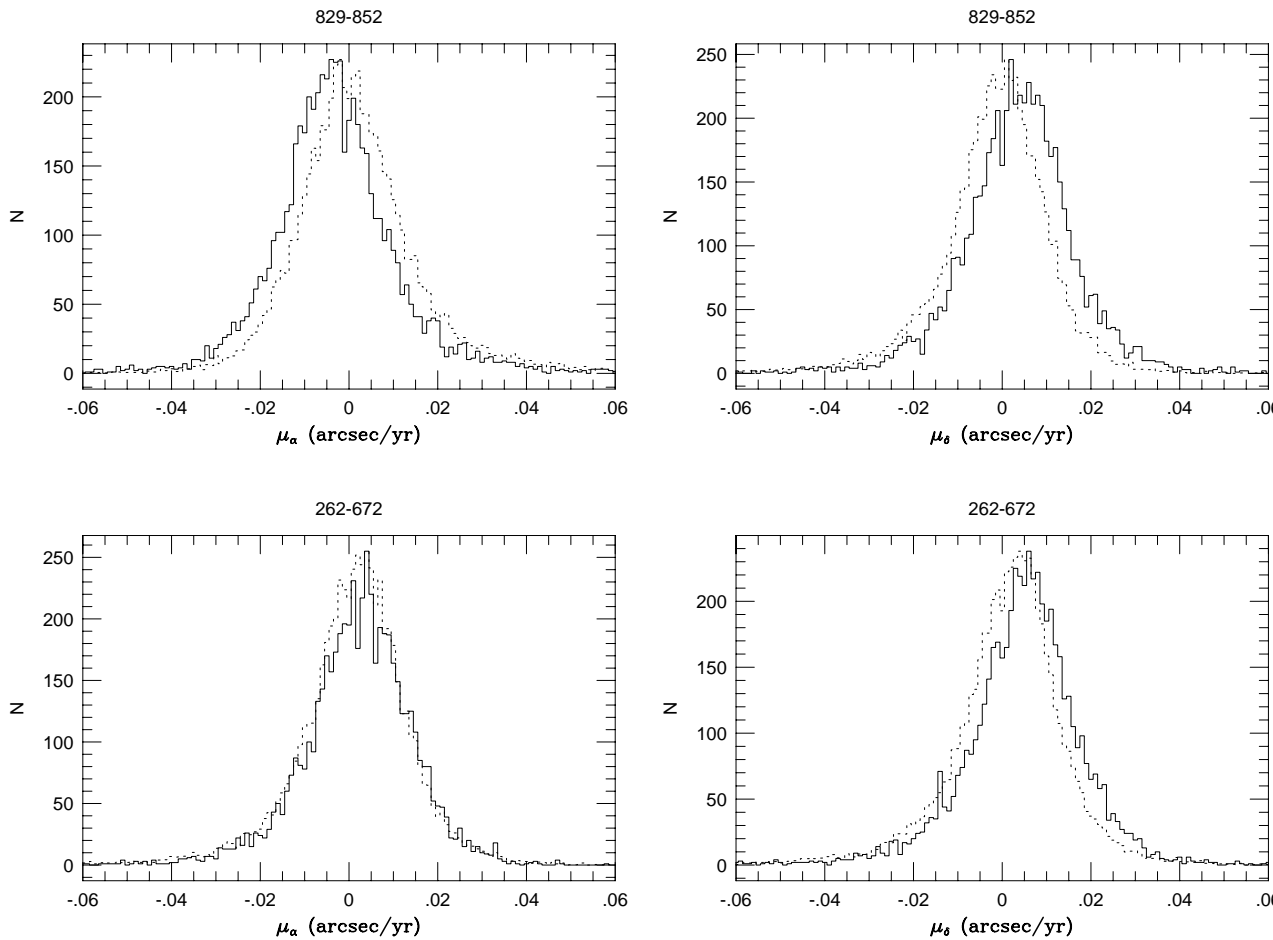


Fig. 2.— Comparison of magnitudes for matches within 3 arcsec for the POSSII field 513 and POSSI plate E102. The outlier points are due to galaxies and merged sources which are treated differently by the two measuring machines.

Fig. 3.— Measured relative proper motions for galaxies and stars. The amplitude of the stellar histograms have been scaled down by a factor of ~ 100 . The median of the galaxy distribution defined the correction to absolute proper motions.



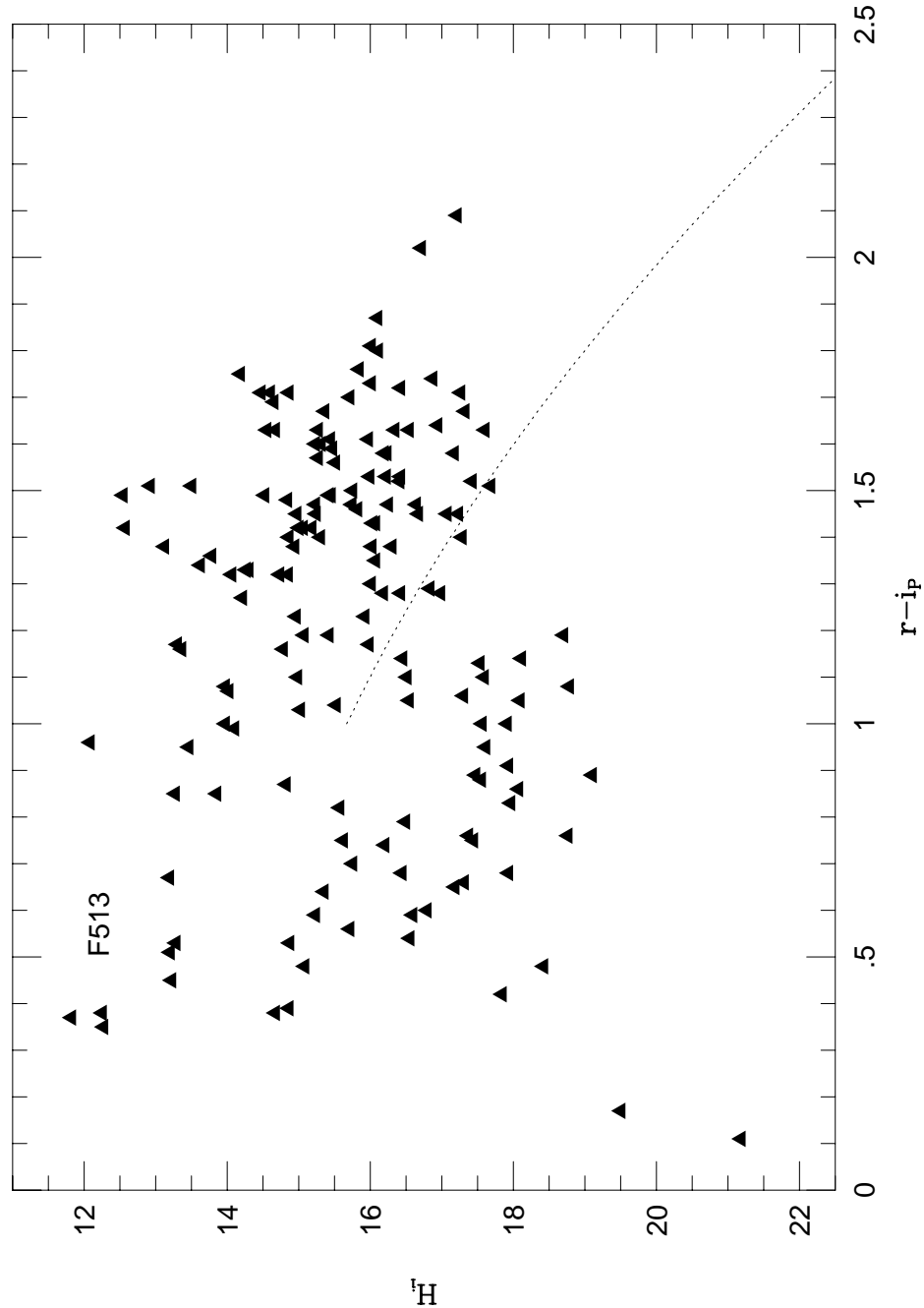


Fig. 4.— The reduced proper motion diagram for Field 513. Halo stars lie below the dotted line, which corresponds to 220 km s^{-1} for near-solar metallicity disk stars.

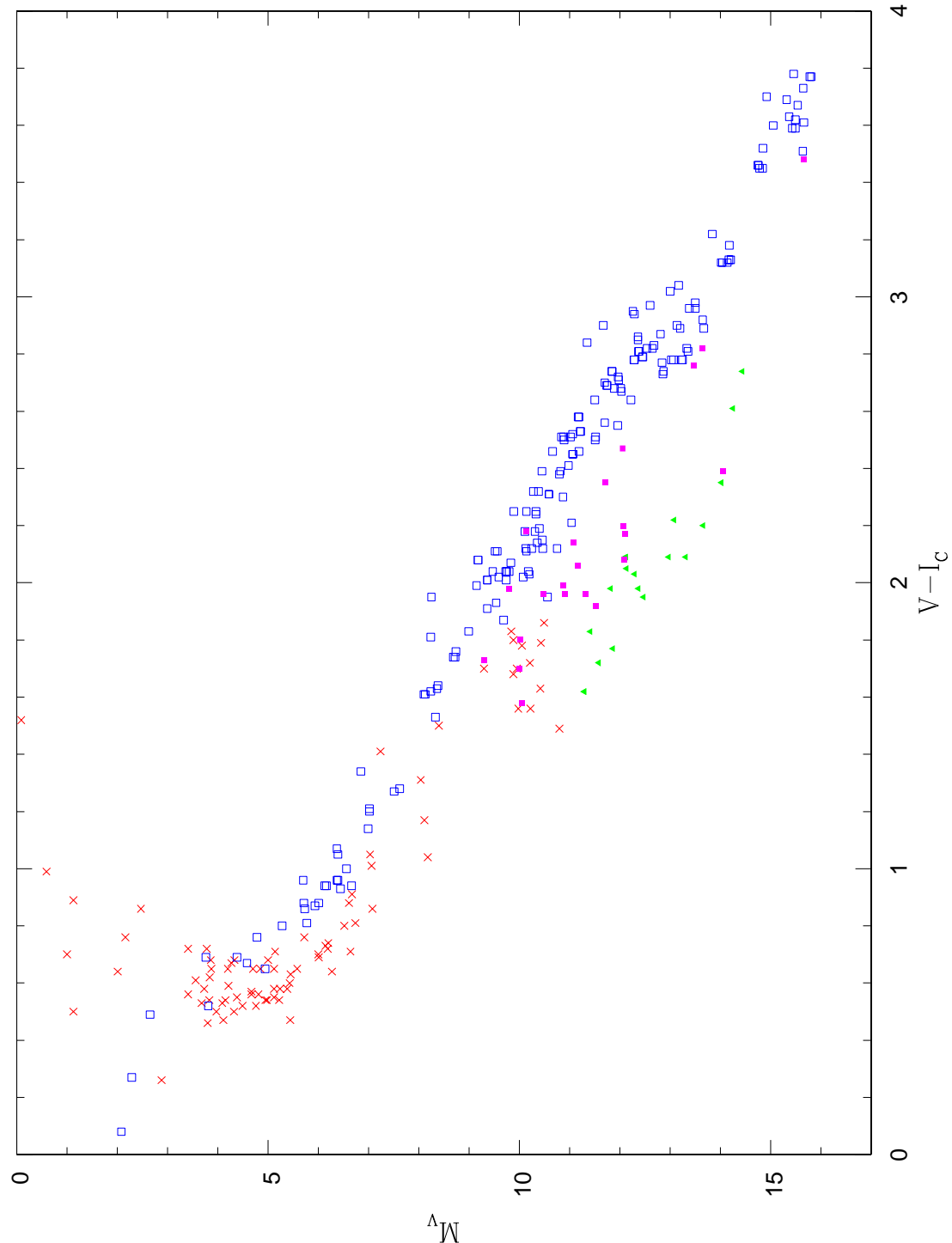


Fig. 5.— The HR Diagram for stars using trigonometric parallaxes. Crosses are stars earlier than type M with $v_{tan} > 220$ km s⁻¹ from the Yale Parallax Catalog (van Altena et al. 1995) or the Hipparcos Catalog, solid squares are sdM (Chapter 2), and solid triangles are esdM. The disk sequence is shown using nearby stars (open squares)

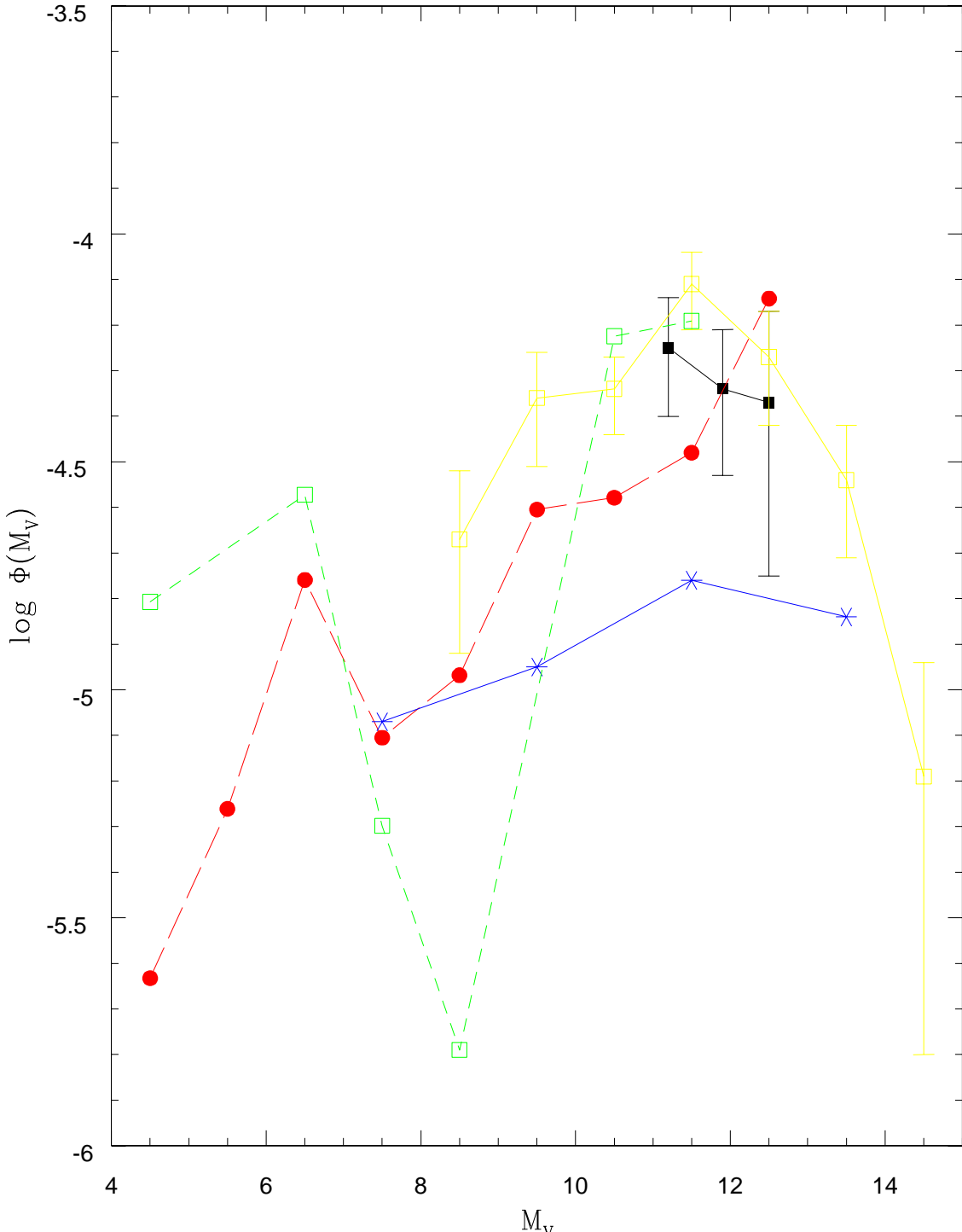


Fig. 6.— Comparison of our halo luminosity function with previously published halo V-band luminosity functions. Our luminosity functions, measured in M_I have been transformed to $\Phi(M_V)$ using Equations 12 (esdM) and 11 (sdM) and then added together (solid squares). The luminosity functions shown are Schmidt (1975, open squares with dashed line), Bahcall & Casertano (1986, solid circles with long-dashed line), Dahn et al. (1995, open squares with solid line), and Gould et al. (1998, asterisks). Note that our luminosity function supports the higher value measured for local LHS stars by Dahn et al. rather than the lower value

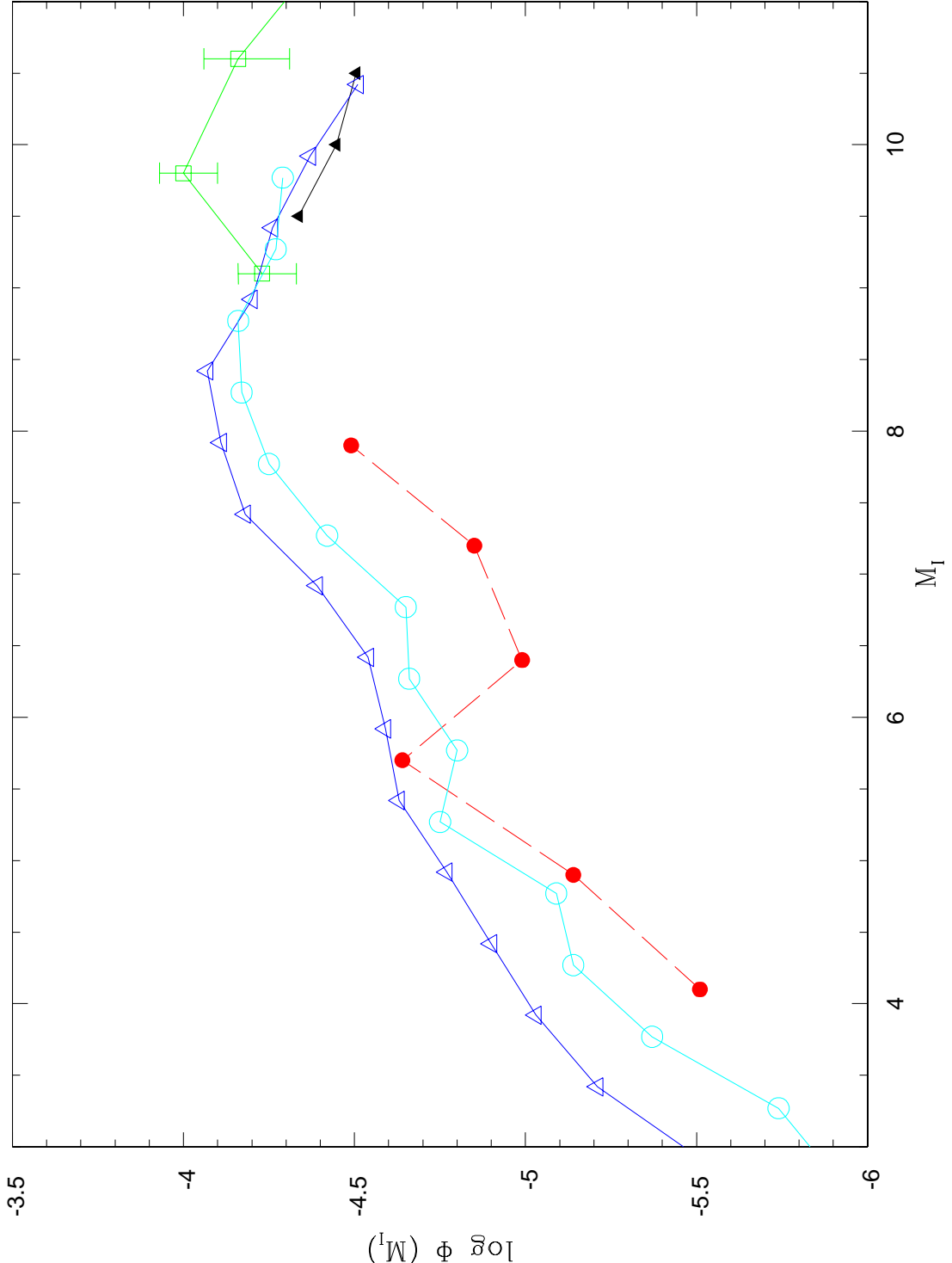


Fig. 7.— The globular clusters NGC 6341 (open triangles) and NGC 7099 (open circles) compared to the esdM luminosity function (solid triangles), Dahn et al. (open squares), and Bahcall & Casertano (solid circles). The BC luminosity functions has been transformed to $\Phi(M_I)$, no account has been taken of any metallicity spread; BC's original kinematic correction has been applied. Correcting for the latter two effects would shift the BC luminosity function downwards. When the globular clusters are normalized to our luminosity function, their luminosity is parallel to but above the BC luminosity function for brighter stars.

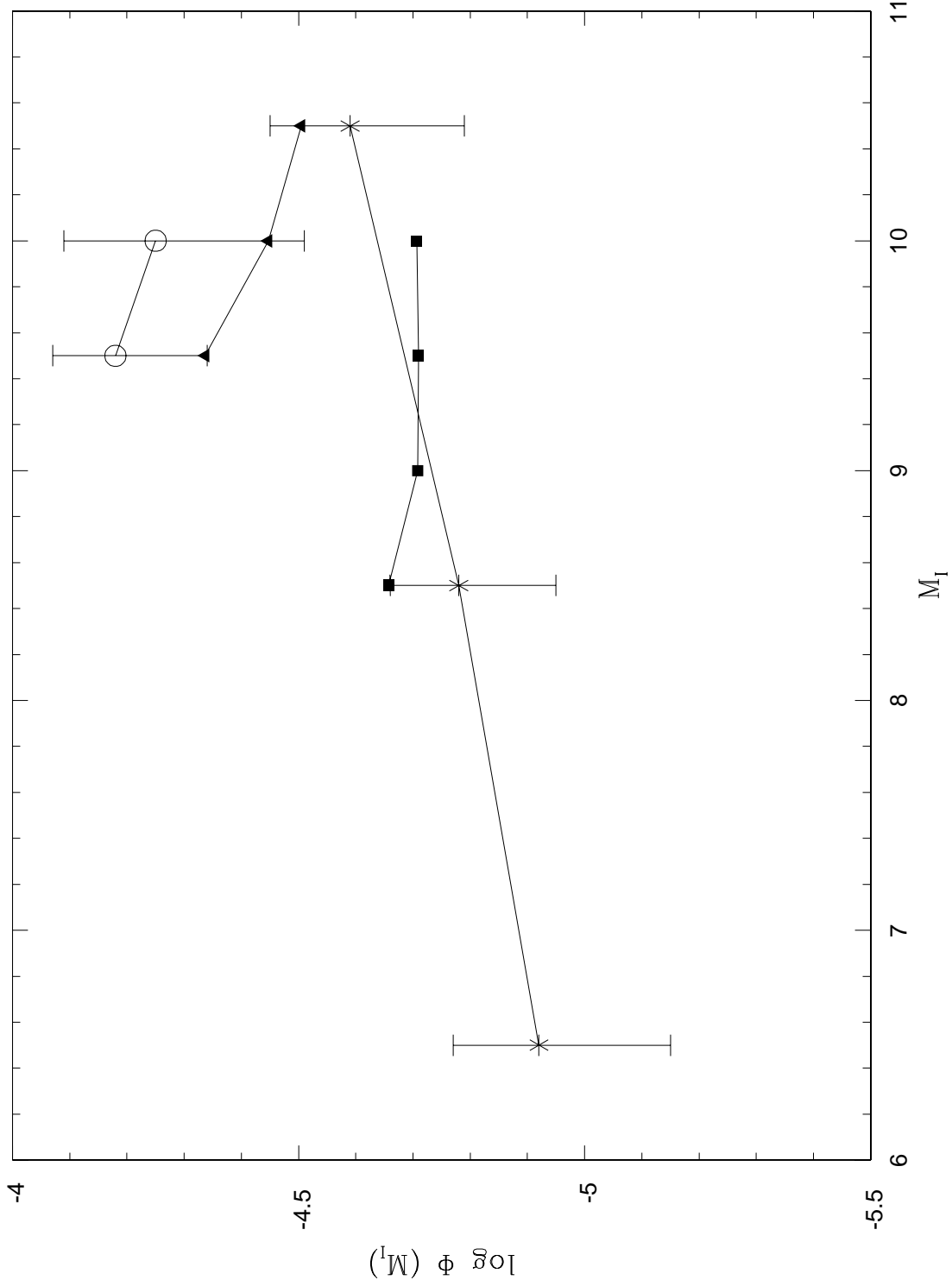


Fig. 8.— Our estimated luminosity function for sdM (solid triangles), esdM (solid squares), and both combined (open squares). Also shown is the Gould et al. HST luminosity function (asterisks). Due to crowding, the error bars have been suppressed for the individual esdM and sdM datasets. It is clear that the HST luminosity function predicts substantially fewer stars than are actually seen.

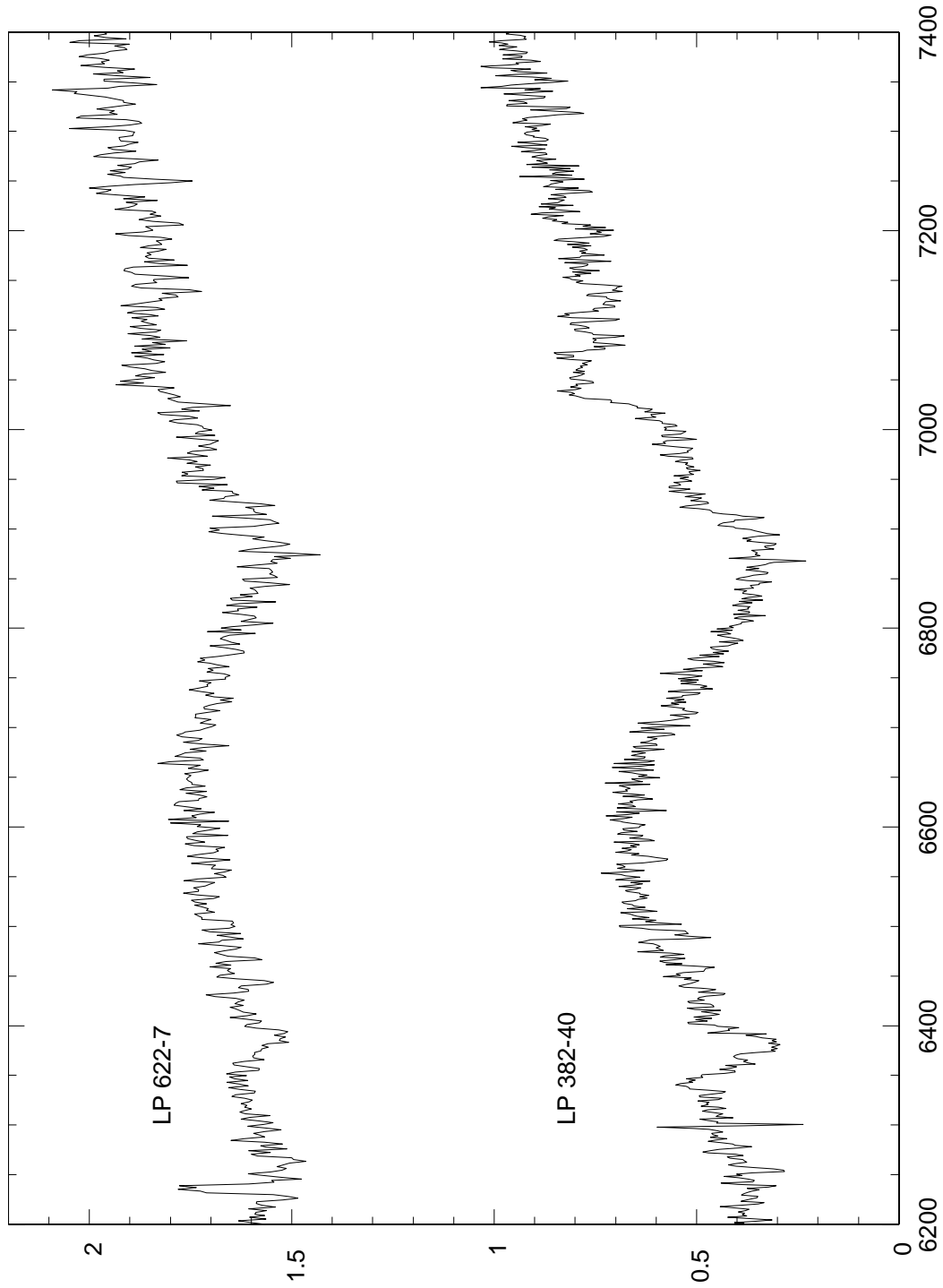


Fig. 9.— The nearby subdwarfs LP 622-7 and LP 382-40. The apparent emission lines at the blue end of the spectra are due to cosmic rays.

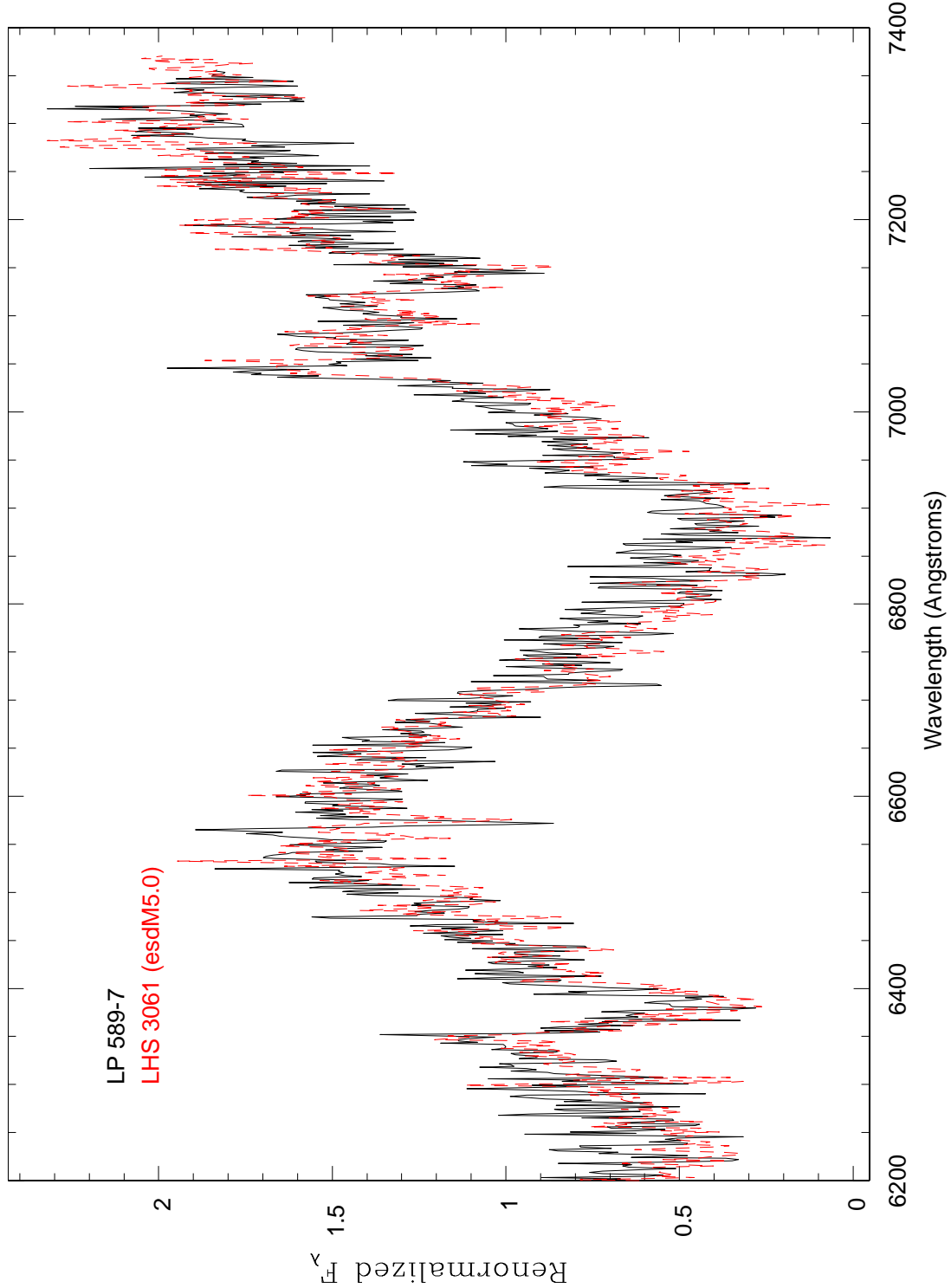


Fig. 10.— The nearby subdwarf LP 589-7 is nearly identical to LHS 3061. Both are classified as esdM5.0 using the Gizis (1997) system. Note the TiO absorption in both stars at 7050\AA , which distinguishes them from the other known esdM5.0 star, LHS 205a.